PCCP

Accepted Manuscript




ROYAL SOCIETY OF CHEMISTRY

www.rsc.org/pccp

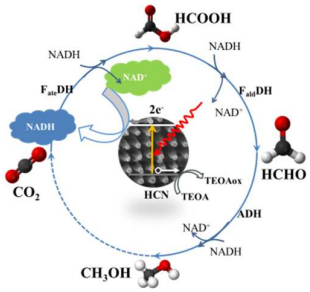


Diatom-inspired, hierarchical carbon nitride materials have been synthesized and used for biophotocatalytic cascade enzymatic conversion of $CO_2$ to methanol.

# Bioinspired construction of ordered carbon nitride array for photocatalytic mediated enzymatic reductions

Jian Liu[a*], Rémi Cazelles[b], Zu Peng Chen[a], Han Zhou[a], Anne Galarneau[b], and Markus Antonietti[a]

[a]*Department of Colloid Chemistry, Max Planck Institute of Colloids and Interfaces, 14424 Potsdam, Germany*

[b]*Institut Charles Gerhardt Montpellier, UMR 5253 CNRS/UM2/ENSCM/UM1, ENSCM, 8 rue de l'Ecole Normale, 34296 Montpellier Cedex 5, France*

[*]Corresponding author. Department of Colloid Chemistry, Max Planck Institute of Colloids and Interfaces, 14424 Potsdam, Germany. Tel,: +49 331 567 9515; fax: +49 331 567 9502.

E-Mail address: Jian.Liu@mpikg.mpg.de

*Keywords:* Bioinspired; Diatom; NADH regeneration; Carbon nitride; photocatalysis

Abstract

Carbon nitride array (CNA) materials have been constructed using a sacrificial diatom template. A regular carbon nitride nanorod array could be replicated from the periodic and regular nanochannel array of the template. The directional charge transport property and high capability for light harvesting of the CNA gives much better performance in splitting water into hydrogen than its bulky counterpart. Furthermore, by combining with a Rhodium complex as mediator, the cofactor NADH of many enzymes could be photocatalytically regenerated by the CNA. The rate of the in-situ NADH regeneration is high enough to reverse the biological pathway of the three dehydrogenase enzymes which then undergoes sustainable conversion of formaldehyde to methanol and also the reduction of carbon dioxide into methanol.

## Introduction

In recent years, substantial efforts both from academic and industrial society have been directed towards the development of high efficiency energy conversion systems turning solar light into chemicals.[1] Material and structure optimization are the key points determining the efficiency of light energy conversion in the artificial systems.[2-3] Biological materials are endless fountainheads of inspirations for the design and fabrication of such kind of nanostructured materials.[4-7] In natural photosynthesis, green plants and algae can

transform carbon dioxide and water into sugars by utilizing light energy and release oxygen into atmosphere. A wide range of nanomaterials have been designed and synthesized using biomaterials or bioinspired processes. The silica exoskeletons (frustules) of the single-celled algae called diatoms are one of the most spectacular examples of biologically evolved nanostructured materials.[8-9] The diatom frustule features the unique architectures with hierarchical structures ranging from micrometric to nanometric scales, which are thought to contribute to their high photosynthesis efficiency.[10-11] Each frustule possesses porous skeleton with regular and periodic pattern, as illustrated in **Scheme 1**.[12] Imitating the ultrastructures of diatom frustule and reconstructing the frustules with photoactive materials could be promising for light energy conversion purpose.[13-14]

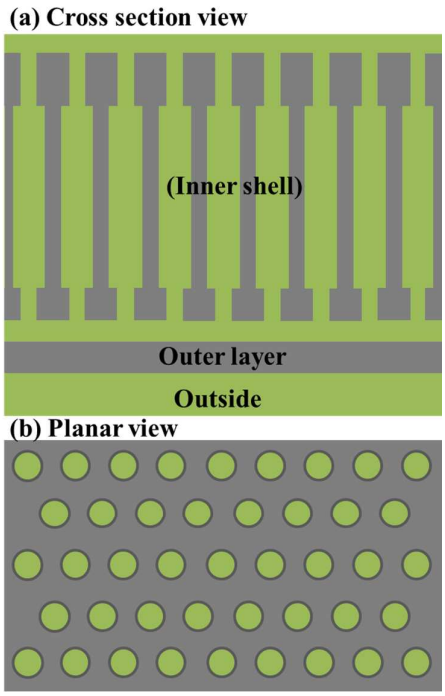


**Scheme 1.** Schematic illustration of inner shell and outer layer structures of diatom.

One dimensional semiconductor nanomaterial (nanorod, nanotube, nanowire) arrays have attracted enormous attention in light energy conversion field due to the potentially facile charge separation and enhanced light absorbance properties.[15-20] These merits have been demonstrated in $TiO_2$ based materials but are to be explored in other visible-light-driven materials, such as graphitic carbon nitride. In recent years, graphitic carbon nitride was found to be a metal-free semiconductor material and meanwhile finds enormous

applications in catalysis, photocatalysis, and bio-related application due to its abundance, high thermal and chemical stability, and visible-light-driven responsive properties.[21-24] Various strategies have been proposed for further improving carbon nitride photocatalysis towards practical purposes.[24-32] However, there are few reports on constructing the carbon nitride array derived from biological materials, which would be promising for light energy conversion, including photocatalytic hydrogen evolution from water and nicotinamide adenine dinucleotide (NADH) regeneration, a necessary coenzyme involved in many biological processes.

In this work, carbon nitride array material (CNA) was prepared by replicating diatom frustules. The Pt nanoparticles decorated CNA exhibited improved hydrogen evolution from water in the presence of triethanolamine compared with bulky carbon nitride. In addition, NADH, the biological form of hydrogen, could be photocatalytically regenerated from $NAD^+$, which allows reversing the biological pathway of dehydrogenase enzymes. In metabolism, NADH/$NAD^+$ is involved in redox reactions, carrying electrons from one reaction to another. Maintaining a kinetically efficient cycle between $NAD^+$ and NADH is extremely important for sustainable dehydrogenase enzymatic reactions.[33-35] The photocatalytic NADH regeneration suggests great possibilities for using light to drive various enzymatic reactions. In-situ regeneration of the cofactor NADH coupled with the yeast alcohol dehydrogenase enzyme (YADH) for the sustainable production of methanol from formaldehyde was realized, as an important step toward enzymatic cascade conversion of $CO_2$ to methanol.[36-37] The work reported here to our opinion could provide a basic and general platform to construct artificial bio-inspired light energy conversion systems from sustainable biological materials.

## Experimental

*Materials*

Formate dehydrogenase ($F_{ate}DH$), Formaldehyde dehydrogenase ($F_{ald}DH$), Yeast alcohol dehydrogenase (YADH), β-Nicotinamide adenine dinucleotide (β-$NAD^+$), reduced nicotinamide adenine dinucleotide

(NADH), Celpure p100 diatomite, Cyanamide, triethanolamine (TEOA), Rhodium(III) chloride hydrate, 2,2'-Bipyridyl, and 1,2,3,4,5-Pentamethylcyclopentadiene were purchased from Sigma-Aldrich.

*Samples fabrication and characterization*

CNA was synthesized through a solid "impregnation incipient wetness" method. 0.5 g of cyanamide and 0.5 g of purified Celpure P100 diatomite was mixed evenly in the mortar and transferred into the crucibles with lid and heated under $N_2$ atmosphere to 600°C (4 hours) and kept at the temperature for another 4 hours. The resultant yellow powder is treated with 4 M $NH_4HF_2$ solution with stirring for 48 hours (**Be cautious!!!**). The dispersion is then filtered; the precipitate is copiously rinsed with deionized water and ethanol. After filtering procedure, the yellow powder is dried under vacuum at 60 °C overnight.

$[Cp^*Rh(bpy)H_2O]^{2+}$ was synthesized as follows: $RhCl_3 \cdot H_2O$ is refluxed in methanol with one equivalent of 1,2,3,4,5-Pentamethylcyclopentadiene for 24 h. The resulting red precipitate is filtrated and suspended in methanol. On addition of two equivalents of 2,2-bipyridine, the suspension clears up immediately and a yellowish solution is formed. $[Cp^*Rh(bpy)Cl]Cl$ is precipitated on the addition of diethyl ether into the obtained yellowish solution. Stock solutions (100 mM) are prepared in water and stored at room temperature avoiding direct light exposure. $[Cp^*Rh(bpy)Cl]Cl$ readily hydrolyzes to $[Cp^*Rh(bpy)(H_2O)]^{2+}$.

XRD measurements were performed on a D8 Diffractometer from Bruker instruments (Cu Kα radiation, λ = 0.154 nm) equipped with a scintillation counter. $N_2$ sorption experiments were done with a Quantachrome Autosorb-1 at liquid nitrogen temperature. TEM images were taken on Philips CM200 FEG (Field Emission Gun), operated at an acceleration voltage of 200 kV. SEM measurement was performed on a LEO 1550 Gemini instrument. The UV-Vis absorbance spectra were recorded on a T70 UV/Vis spectrophotometer.

*Photocatalytic water splitting by CNA*

In a typical experiment, 50 mg carbon nitride material was placed in the photoreactor (equipped with a magnetic stirrer) then the reactor was evacuated and refilled with argon for five times. Then 38 mL of aqueous TEOA solution (10 vol% TEOA) containing the platinum precursor (Pt metal content: 3% weight of carbon nitride) was added under argon flow. The set-up is equipped with a thermostat and stirring plate. $H_2O$ and TEOA were pretreated before use. $H_2O$ was firstly degassed for 1 h under vacuum in an ultrasonic bath and secondly purged with argon for 1 h. TEOA was purged for 1 h with argon. After the reaction, a sample of the headspace was analyzed with GC for hydrogen content.

*Photocatalytic regeneration of NADH and enzymatic reactions*

In a typical regeneration procedure, the reaction medium was composed of $NAD^+$ (1 mM), TEOA (15 w/v%), phosphate buffer (100 mM) and CNA (3 mg). The reaction system was placed into a quartz reactor

equipped with stirring bar and illuminated with LED lamp (wavelength=420 nm, OSA Opto Light GmbH). The distance between reactor and LED lamp is fixed at 5.5 cm. During the illumination, the concentration of NADH was estimated by measuring the absorbance of diluted reaction system at 340 nm. $NAD^+$ has peak absorption at a wavelength of 260 nm, with an extinction coefficient of 16,900 $M^{-1}\cdot cm^{-1}$. NADH has peak absorption at 340 nm with an extinction coefficient of 6,220 $M^{-1}\cdot cm^{-1}$.

The conversion of formaldehyde to methanol was performed in quartz reactor. The reaction solution was composed of 3 mg CNA, $NAD^+$ (1 mM), **M** (0.125 mM), formaldehyde solution (5 mM), Alcohol dehydrogenase (0.45 mg) in 3 ml 0.1 M PBS buffer (pH=7.0). Prior to the addition of enzyme stock solution, the PBS buffer was firstly saturated with Nitrogen. The amount of methanol was detected by GC.

The conversion of $CO_2$ to methanol was performed in quartz reactor. The reaction solution was composed of 3 mg CNA, NADH (1 mM), $KHCO_3$ (0.1M), **M** (0.125 mM), Formate dehydrogenase(0.02 mg), Formaldehyde dehydrogenase (0.3 mg) Alcohol dehydrogenase (1.5 mg) in 2 ml 0.1 M PBS buffer (pH=7.0). Prior to the addition of enzyme stock solution, the PBS buffer was firstly saturated with gaseous $CO_2$. The amount of methanol was detected by GC.

**Results and discussions**

The CNA was synthesized by a simple sacrificial diatom template method.[22, 38] The commercially available diatom frustule was first purified by gravity sedimentation. During the repeated purification and washing process, the smallest fragments of diatoms were removed due to their slower rate of sedimentation. For templating, only the largest fragments (> 20 microns) were used and the major components are large segments with ordered nanochannel arrays corresponding to a final yield of 10 wt% (See **Figure S1** of Supporting Information, abbreviated as SI). The purified diatom template was dried at ambient condition and mechanically mixed together with equal amount of cyanamide in a mortar (See **Figure S2** of SI). The resultant powder was put at 600 ºC in a nitrogen oven for 4 hours for thermal condensation of the carbon nitride network (**Figure S3** of SI). Finally, the resulting homogeneous yellow powder was treated with $NH_4HF_2$ to remove the diatom template, and the hierarchical carbon nitride nanorod array structures were obtained (**Figure 1**). Therefore, the whole process can be summarized as follows: 1) purification and drying

of the diatom frustule; 2) mechanical mixing with cyanamide and high temperature thermal condensation; 3) removal of diatom template.[39]

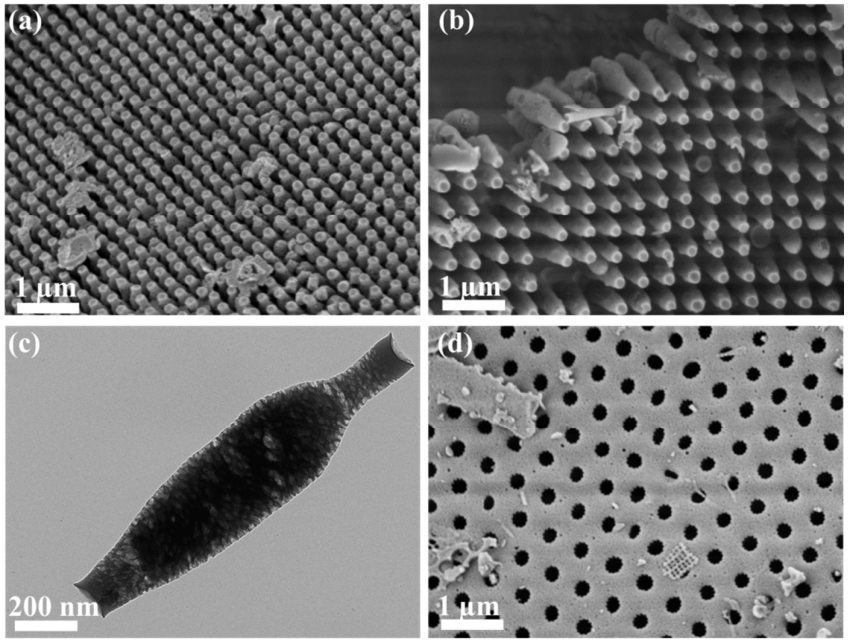


**Figure 1**. SEM images of CNA with the top (a) and the lateral (b) view of the array of carbon nitride nanorods array. (c) TEM image of single carbon nitride nanorod detached from CNA. (d) SEM image of the starting diatom frustule template featuring periodic and regular porous pattern.

Structural details revealed by scanning electron microscopy (SEM) and transmission electron microscopy (TEM) are presented in **Figure 1**. As shown in **Figure 1a**, the carbon nitride nanorods array is maintained even after vigorous stirring during $NH_4HF_2$ treatment process. A lateral view is presented in **Figure 1b** to demonstrate the intact carbon nitride nanorods array. Additional views of CNA are also presented in **Figure S4** of SI. As can be seen from **Scheme 1**, the inner structure of diatoms is a honeycomb structure of pores, which are connected to the external surface by smaller pores. The outer layer plays an important role in maintaining the dense structure of regular nanorods of carbon nitride even after vigorous stirring during template removal process, providing the mechanical robustness of the CNA. The nanorods array is attached to a plane coming from the replica of the outer surface of diatoms and is therefore different and easier to manipulate than discrete nanorods derived from anodic aluminum oxide or silica nanorod.[27] Further looking at a single and intact nanorod sheds some light on the formation mechanism. TEM image of

an intact carbon nitride nanorod is shown in **Figure 1c,** revealing a nanoporous structure with pore size of around 20 nm. It is also interesting to find that the vase-shaped nanorod features a small concave cavity on both ends. It can be speculated that its formation is derived from the non-confined condensation on the ends compared with the nanoconfinment in the interior of the nanochannel, allowing minor shrinking. Both tips of the rod are narrower than the body size, corresponding to the original template. Practically no bulky carbon nitride particles are observed in the CNA sample, demonstrating the cyanamide is exclusively confined in the frustule pore channels. The cyanamide precursor in the evenly mixed solid phase with diatom melt at elevated temperatures and is pulled by capillary forces into the interior of channel and undergoes thermal condensation into graphitic carbon nitride afterwards. TGA analysis (**Figure S5** of SI) demonstrates that only around 1% of silica residue was found to left in the final CNA samples, indicating most of the silica template was successfully removed during etching process.

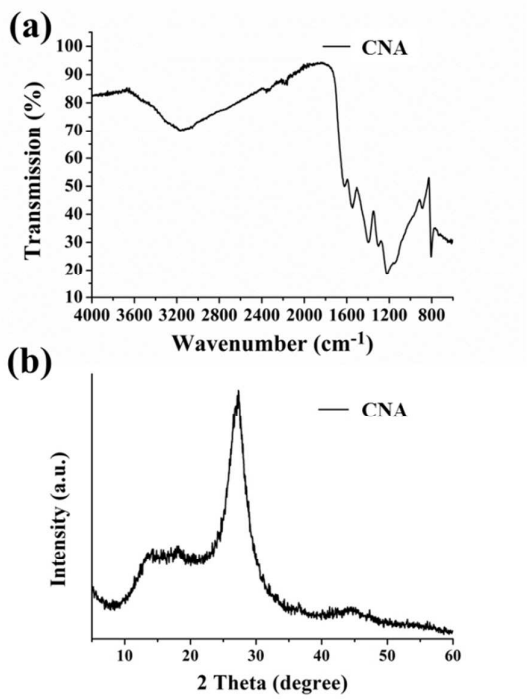


**Figure 2**. a) FTIR spectrum of CNA showing typical C-N heterocycle stretches in the 1100~1600 $cm^{-1}$ spectral range and the breathing mode of the tri-s-triazine units at 810 $cm^{-1}$. (b) XRD spectrum of CNA with two peaks at 13.0º and 27.4º ascribed to the in-planar repeat period and stacking of the conjugated aromatic system, respectively.

The Fourier transform infrared spectroscopy (FTIR) and Powder X-ray diffraction (XRD)

characterizations depicted in **Figure 2** demonstrate the obtained CNA is a typical polymeric graphitic carbon nitride material featuring novel hierarchical structures. The band at 810 $cm^{-1}$ in the FTIR spectrum is ascribed to the s-triazine ring modes, while the bands at 1200~1600 $cm^{-1}$ are characteristics of aromatic CN heterocycles (**Figure 2a**). The XRD shows the two characteristic peaks of graphitic carbon nitride (**Figure 2b**) at 13.0º and 27.4º which are ascribed to the in-planar repeat period and stacking of the conjugated aromatic system, respectively.

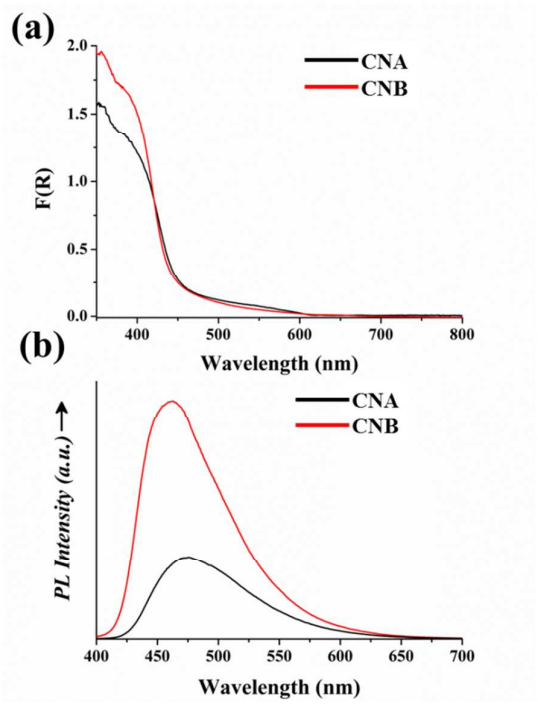


**Figure 3**. (a) Optical absorption and (b) photoluminescence spectra of CNA and CNB, respectively.

The optical property of CNA was measured by UV-vis diffuse reflection spectra (**Figure 3a**). CNA exhibits typical semiconductor absorption in the blue region, similarly as the CNB (bulky carbon nitride). The photogenerated charge carrier separation and recombination were also investigated by photoluminescence spectra under excitation at 380 nm. As shown in **Figure 3b**, the samples exhibit a broad emission peak centering at 470 nm. Compared with the CNB, the fluorescence emission of CNA is greatly decreased, suggesting a suppressed recombination of the photo-induced charge carriers, which is beneficial for further heterogeneous photocatalysis.

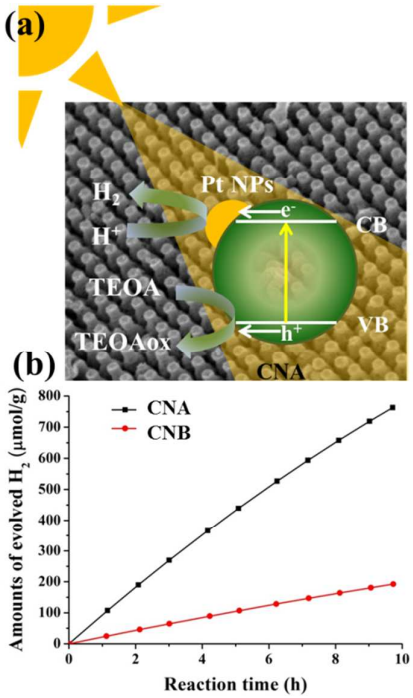


**Figure 4**. (a) Schematic hydrogen evolution by Pt nanoparticles decorated CAN and (b) time courses of $H_2$ evolution rate for CNA and CNB during a 10 hour experiment. CB: Conduction band; VB: Valence band; TEOA: triethanolamine.

CNA was firstly evaluated in a photocatalytic hydrogen evolution activity test by loading 3 wt% Pt as cocatalyst and using triethanolamine (TEOA) as a hole scavenger. Under illumination, the electrons in the valence band are excited to the conduction band. The photoinduced electrons in the conduction band will further migrates to the Pt nanoparticles deposited on the surface of carbon nitride by crossing the aligned Fermi energy levels. The electron vacancy in the valence band will be restored by the TEOA, producing glycolaldehyde and di(ethanol)amine as the oxidizing products. The hydrogen evolution results are presented in **Figure 4**. The performance in photocatalytic water splitting into hydrogen is improved by a factor of 4 over that of CNB. The hydrogen evolution amount increases linearly and hydrogen evolution capability didn't show any obvious decay in the 10 hours run experiment. Considering low surface area for CNA (25 $m^2/g$) compared to CNB (28 $m^2/g$) (**Figure S6** of SI), the higher activity can be attributed to the introduction of the well-ordered nanorod array structure. The directional charge transport properties of the carbon nitride nanorod array together with the multiple light scattering of segmented photocatalyst contribute to the improvement of photocatalytic hydrogen evolution.[40-42]

The photocatalytic property of CNA was also investigated in the biocatalytic conversion of formaldehyde into methanol (selected as test reaction) using Yeast alcohol dehydrogenase enzyme (YADH), which NADH cofactor needs to be regenerated for a sustainable production of methanol. YADHs are enjoying increasing interest as versatile and selective biocatalysts from both academic and industrial fields. The reduction of pro-chiral ketones is an area of application most attractive to organic chemists while the reversible process of the oxidation of alcohols is less attractive due to the destruction of chirality. Usually, for the sustainable enzymatic synthesis of a chiral alcohol, another enzyme, such as formate dehydrogenase and phosphite dehydrogenase, is used to regenerate NADH. A natural photosystem as plant chloroplasts could also be used for NADH regeneration but presents very low stability over time. In order to increase the long term stability and also reduce the complexity of the system, we have investigated the light-driven NADH regeneration by CNA, which is inherently sustainable. We investigated the regeneration of 1,4-NADH from $NAD^+$ by CNA photocatalysis, in the presence of $[Cp^*Rh(bpy)H_2O]^{2+}$ (abbreviated as **M**, see HNMR in **Figure S7** of SI) as an electron mediator and hydride transfer agent. The electrons are transferred to $[Cp^*Rh(bpy)H_2O]^{2+}$ to form Cp*Rh(bpy), followed by coupling with one proton to generate the hydriderhodium $[Cp^*Rh(bpy)H]^+$, which acts as hydride transfer reagent towards NADH regeneration from $NAD^+$. TEOA is employed as sacrificial electron donor. The oxidized state of TEOA provides the protons during its decomposition path to glycolaldehyde and di(ethanol)amine. The NADH concentration gradually increases throughout illumination in the reaction medium, as evidenced from the absorbance peak intensity in the 340 nm wavelength quantified by UV-vis spectrophotometer, shown in **Figure S8** of SI. During the reduction of formaldehyde into methanol, NADH is oxidized into $NAD^+$ and the light energy is used to reduce back $NAD^+$ into NADH. Optimum enzymatic reaction conditions for YADH for the reduction of formaldehyde into methanol were previously determined and the highest activity was obtained for pH values between 5 and 7 in accordance with literature for other reactions. The previously optimized

conditions of reaction were applied for the following photocatalytic regeneration of NADH with CNA.

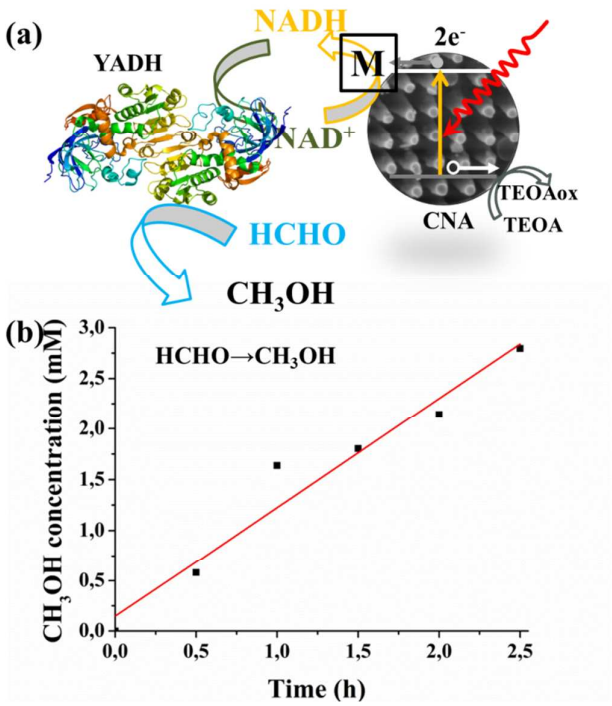


**Figure 5**. (a) Schematic illustration of conversion of formaldehyde into methanol by YADH with NADH regenerated by CNA photocatalysis in the presence of **M**. (b) Production of methanol as a function of time obtained in the biophotocatalytic system.

The CNA based photocatalytic NADH regeneration system was successfully combined with YADH conversion, as illustrated in **Figure 5a**. We proved that the in situ regenerated NADH is in fact useful as a hydride equivalent for the enzymatic reduction. The Rhodium complex mediated NADH regeneration by carbon nitride photocatalysis is obviously also rather efficient. According to the illustrated results, a complete and nearly linear conversion of formaldehyde to methanol was obtained in 3 hours. As a reference experiment, a dark enzymatic reaction gave no detectable methanol. The result for methanol production in solution is shown in **Figure 5b** (0.21 $mmol_{Methanol}/min/g_{enzyme}$). It is thereby demonstrated that the NADH regeneration by carbon nitride photocatalysis plays the energetically driving role in the formaldehyde conversion process.

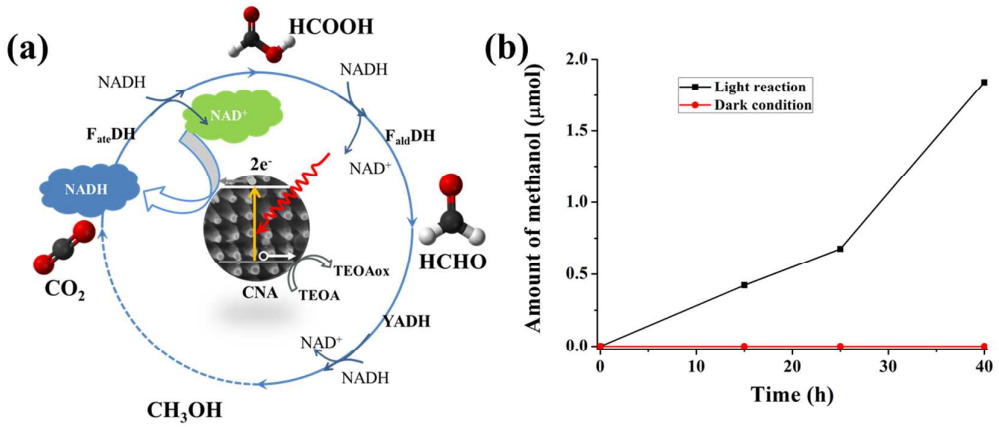


**Figure 6.** (a) Schematic illustration of three consecutive enzymatic reactions for converting $CO_2$ into methanol with in-situ regenerated NADH by CNA photocatalysis; (b) Production of methanol as a function of time obtained in the three enzyme based biophotocatalytic system.

Furthermore, in view of the success of the preliminary transformation of formaldehyde to methanol, the three consecutive enzymatic conversion of $CO_2$ into methanol was consequently tested (**Figure 6a**). The optimized enzymatic powder ratios between the three enzymes were used.[43] $CO_2$ was generated from $NaHCO_3$ (0.1 M). The actual gaseous $CO_2$ dissolved in the pH 7 buffer solution was 8 mM.[44] We performed continuous reduction of $CO_2$ to methanol during 40 hours illumination, 1.8 μmol of methanol was produced corresponding to a productivity of 0.07 $mmol_{MeOH}/g_{enzymes}$ in 3 hours (**Figure 6b**). We can observe the approximately linear increase of methanol yield as the illumination time increases. Meanwhile, the dark enzymatic reaction does not produce any methanol. Therefore, the NADH regeneration by the photosynthetic material is effective enough to reverse the natural reaction pathway of the three dehydeogenase enzymes. Enzymatic conversion of $CO_2$ to methanol with the photocatalytic NADH regeneration is therefore firstly proven feasible. The capability of carbon nitride material for NADH regeneration has been compared to a biological system using the phosphite dehydrogenase enzyme. Some of the current authors obtained a productivity of 0.16 $mmol_{MeOH}/g_{enzymes}$ in 3 hours but using a pressure of 5 bars of $CO_2$ thus allowing the dissolution of 5 times more $CO_2$ in aqueous media.[43] The conversion efficiency of our current system can still be enhanced by using a suitable pressurized photocatalytic reactor.

## Conclusions

In summary, diatom-inspired, hierarchical carbon nitride materials have been synthesized and used for biophotocatalytic enzymatic conversion of formaldehyde to methanol as well as splitting water into hydrogen. The work reported here to our opinion provides a general and basic platform to construct bio-inspired artificial light energy conversion systems.[45] Future work might involve coupling the carbon nitride photocatalytic regeneration system with enzyme immobilization within the confinement of mesopores in the carbon nitride matrix. It would substantially improve the enzyme stability for long term uses and also large scale applications.[46] Furthermore, it is exciting to inquire the diversity of diatom species to retro-analyze other structures for their efficiency in artificial photosynthesis. Finally, we proved that synthetic phostosystems are suitable for the regeneration of the biologically active NADH cofactor in biophotosynthetic processes.

**Acknowledgements**

J. Liu acknowledges the support of Alexander von Humboldt Foundation and helpful assistance and discussion by Dr. Hongqiang Wang of MPIKG. H. Zhou acknowledges the financial support by the National Natural Science Foundation of China (51102163).

**References**

(1) Woolerton, T. W.; Sheard, S.; Reisner, E.; Pierce, E.; Ragsdale, S. W.; Armstrong, F. A., *J. Am. Chem. Soc.* **2010**, *132*, 2132-2133.

(2) Huang, J.; Antonietti, M.; Liu, J., *J. Mater. Chem. A*, **2014**, Doi: 10.1039/C4TA00793J.

(3) Liu, J.; Liu, G.; Li, M.; Shen, W.; Liu, Z.; Wang, J.; Zhao, J.; Jiang, L.; Song, Y., *Energy Environ. Sci.* **2010**, *3*, 1503-1506.

(4) Parker, A. R.; Townley, H. E., *Nat. Nanotechnol.* **2007**, *2*, 347-353.

(5) Nadine, N.; Jacques, L., *Chem. Soc. Rev.* **2011**, *40*, 849-859.

(6) Kubacka, A.; Fernández-García, M.; Colón, G., *Chem. Rev.* **2011**, *112*, 1555-1614.

(7) Liu, J.; Yang, Q.; Yang, W.; Li, M.; Song, Y., *J. Mater. Chem. A* **2013**, *1*, 7760-7766.

(8) Sumper, M.; Brunner, E., *Adv. Funct. Mater.* **2006**, *16*, 17-26.

(9) Zhang, H.; Shahbazi, M.-A.; Mäkilä, E. M.; da Silva, T. H.; Reis, R. L.; Salonen, J. J.; Hirvonen, J. T.; Santos, H. A., *Biomaterials* **2013**, *34*, 9210-9219.

(10) Losic, D.; Mitchell, J. G.; Lal, R.; Voelcker, N. H., *Adv. Funct. Mater.* **2007**, *17*, 2439-2446.

(11) Fuhrmann, T.; Landwehr, S.; El Rharbi-Kucki, M.; Sumper, M., *Appl. Phys. B: Lasers Opt.* **2004**, *78*, 257-260.

(12) Bao, Z.; Weatherspoon, M. R.; Shian, S.; Cai, Y.; Graham, P. D.; Allan, S. M.; Ahmad, G.; Dickerson, M. B.; Church, B. C.; Kang, Z., *Nature* **2007**, *446*, 172-175.

(13) Jeffryes, C.; Campbell, J.; Li, H.; Jiao, J.; Rorrer, G., *Energy Environ. Sci.* **2011**, *4*, 3930-3941.

(14) Zhou, H.; Fan, T.; Li, X.; Ding, J.; Zhang, D.; Li, X.; Gao, Y., *Eur. J. Inorg. Chem.* **2009**, *2009*, 211-215.

(15) Ye, M.; Gong, J.; Lai, Y.; Lin, C.; Lin, Z., *J. Am. Chem. Soc.* **2012**, *134*, 15720-15723.

(16) Mor, G. K.; Shankar, K.; Paulose, M.; Varghese, O. K.; Grimes, C. A., *Nano Lett.* **2005**, *5*, 191-195.
(17) Zhu, K.; Neale, N. R.; Miedaner, A.; Frank, A. J., *Nano Lett.* **2007**, *7*, 69-74.
(18) Zhang, J.; Wang, Y.; Jin, J.; Zhang, J.; Lin, Z.; Huang, F.; Yu, J., *ACS Appl. Mater. Interfaces* **2013**, 10317-10324.
(19) Jiu, J.; Isoda, S.; Wang, F.; Adachi, M., *J. Phys. Chem. B* **2006**, *110*, 2087-2092.
(20) Peng, K. Q.; Lee, S. T., *Adv. Mater.* **2011**, *23*, 198-215.
(21) Wang, X.; Maeda, K.; Thomas, A.; Takanabe, K.; Xin, G.; Carlsson, J. M.; Domen, K.; Antonietti, M., *Nat. Mater.* **2008**, *8*, 76-80.
(22) Wang, Y.; Wang, X.; Antonietti, M., *Angew. Chem., Int. Ed.* **2012**, *51*, 68-89.
(23) Zhang, J.; Zhang, G.; Chen, X.; Lin, S.; Möhlmann, L.; Dołęga, G.; Lipner, G.; Antonietti, M.; Blechert, S.; Wang, X., *Angew. Chem.* **2012**, *124*, 3237-3241.
(24) Zhang, J.; Chen, X.; Takanabe, K.; Maeda, K.; Domen, K.; Epping, J. D.; Fu, X.; Antonietti, M.; Wang, X., *Angew. Chem., Int. Ed.* **2010**, *49*, 441-444.
(25) Chen, X.; Jun, Y.-S.; Takanabe, K.; Maeda, K.; Domen, K.; Fu, X.; Antonietti, M.; Wang, X., *Chem. Mater.* **2009**, *21*, 4093-4095.
(26) Cui, Y.; Ding, Z.; Fu, X.; Wang, X., *Angew. Chem., Int. Ed.* **2012**, *51*, 11814-11818.
(27) Li, X.-H.; Zhang, J.; Chen, X.; Fischer, A.; Thomas, A.; Antonietti, M.; Wang, X., *Chem. Mater.* **2011**, *23*, 4344-4348.
(28) Liu, J.; Antonietti, M., *Energy Environ. Sci.* **2013**, *6*, 1486-1493.
(29) Yang, S.; Gong, Y.; Zhang, J.; Zhan, L.; Ma, L.; Fang, Z.; Vajtai, R.; Wang, X.; Ajayan, P. M., *Adv. Mater.* **2013**, *25*, 2452-2456.
(30) Zhang, Y.; Schnepp, Z.; Cao, J.; Ouyang, S.; Li, Y.; Ye, J.; Liu, S., *Sci. Rep.* **2013**, *3*, 2163.
(31) Jun, Y. S.; Park, J.; Lee, S. U.; Thomas, A.; Hong, W. H.; Stucky, G. D., *Angew. Chem., Int. Ed.* **2013**, *52*, 11083-11087.
(32) Niu, P.; Zhang, L.; Liu, G.; Cheng, H. M., *Adv. Funct. Mater.* **2012**, *22*, 4763-4770.
(33) Choudhury, S.; Baeg, J. O.; Park, N. J.; Yadav, R. K., *Angew. Chem., Int. Ed.* **2012**, *124*, 11792-11796.
(34) Ryu, J.; Lee, S. H.; Nam, D. H.; Park, C. B., *Adv. Mater.* **2011**, *23*, 1883-1888.
(35) Könst, P.; Merkens, H.; Kara, S.; Kochius, S.; Vogel, A.; Zuhse, R.; Holtmann, D.; Arends, I. W.; Hollmann, F., *Angew. Chem., Int. Ed.* **2012**, *51*, 9914-9917.
(36) Obert, R.; Dave, B. C., *J. Am. Chem. Soc.* **1999**, *121*, 12192-12193.
(37) Xu, S.-w.; Lu, Y.; Li, J.; Jiang, Z.-y.; Wu, H., *Ind. Eng. Chem. Res.* **2006**, *45*, 4567-4573.
(38) Goettmann, F.; Fischer, A.; Antonietti, M.; Thomas, A., *Angew. Chem., Int. Ed.* **2006**, *45*, 4467-4471.
(39) Liu, J.; Huang, J.; Dontosova, D.; Antonietti, M., *RSC Adv.* **2013**, *3*, 22988-22993.
(40) Xiong, F.-Q.; Wei, X.; Zheng, X.; Zhong, D.; Zhang, W.; Li, C., *J. Mater. Chem. A* **2014**, *2*, 4510-4513.
(41) Maijenburg, A. W.; Rodijk, E. J.; Maas, M. G.; Enculescu, M.; Blank, D. H.; ten Elshof, J. E., *Small* **2011**, *7*, 2709-2713.
(42) Liu, Y.; Wang, H.; Wang, Y.; Xu, H.; Li, M.; Shen, H., *Chemical Communications* **2011**, *47*, 3790-3792.
(43) Cazelles, R.; Drone, J.; Fajula, F.; Ersen, O.; Moldovan, S.; Galarneau, A., *New J. Chem.* **2013**, *37*, 3721-3730.
(44) Duan, Z.; Sun, R., *Chem. Geol.* **2003**, *193*, 257-271.
(45) Yadav, R. K.; Baeg, J.-O.; Oh, G. H.; Park, N.-J.; Kong, K.-J.; Kim, J.; Hwang, D. W.; Biswas, S. K., *J. Am. Chem. Soc.* **2012**, *134*, 11455–11461.
(46) Zhou, Z.; Hartmann, M., *Chem. Soc. Rev.* **2013**, *42*, 3894-3912.